Spin injection from Fe into Si(001): *Ab initio* calculations and role of the Si complex band structure

Phivos Mavropoulos
Institut für Festkörperforschung and Institute for Advanced Simulations, Forschungszentrum Jülich , D-52425 Jülich, Germany
(Received 8 July 2008; published 27 August 2008)

We study the possibility of spin injection from Fe into Si(001), using the Schottky barrier at the Fe/Si contact as tunneling barrier. Our calculations are based on density-functional theory for the description of the electronic structure and on a Landauer-Büttiker approach for the current. The current-carrying states correspond to the six conduction-band minima (pockets) of Si, which, when projected on the (001) surface Brillouin zone (SBZ), form five conductance hot spots: one at the SBZ center and four symmetric satellites. The satellites yield a current polarization of about 50%, while the SBZ center can, under very low gate voltage, yield up to almost 100%, showing a zero-gate anomaly. This extremely high polarization is traced back to the symmetry mismatch of the minority-spin Fe wave functions to the conduction-band wave functions of Si at the SBZ center. The tunneling current is determined by the complex band structure of Si in the [001] direction, which shows qualitative differences compared to that of direct-gap semiconductors. Depending on the Fermi level position and Schottky barrier thickness, the complex band structure can cause the contribution of the satellites to be orders of magnitude higher or lower than the central contribution. Thus, by appropriate tuning of the interface properties, there is a possibility to cut off the satellite contribution and to reach high injection efficiency. Also, we find that a moderate strain of 0.5% along the [001] direction is sufficient to lift the degeneracy of the pockets so that only states at the zone center can carry current.

DOI: 10.1103/PhysRevB.78.054446 PACS number(s): 72.25.Hg, 85.75.−d

I. INTRODUCTION

The electrical injection of spin-polarized carriers, for short called *electrical spin injection*, into the conduction band of semiconductors is one of the key elements for realizing spin transistors such as the one proposed by Datta and Das.[1] Following arguments by Schmidt and coworkers,[2] Rashba,[3] and Fert and Jaffrès,[4] it was realized that efficient spin injection requires the presence of a tunnel barrier at the ferromagnet/semiconductor interface. Significant experimental success started in 2001–2002,[5] in junctions that contained a tunnel barrier between the ferromagnetic metal and the semiconductor, either in the form of the Schottky barrier of the semiconductor itself or in the form of an ultrathin film of some other insulating material,[6] such as AlO or MgO.[7] Most works have focused on injection into GaAs,[5–8] where the current polarization can be detected optically in GaAs/AlGaAs/GaAs quantum wells or electrically in lateral-geometry experiments.[8] Recently, however, electrical spin injection into Si has also been demonstrated via electrical spin detection,[9–12] nonlocal electrical detection,[12] and optical detection,[13] with impressively large spin coherence length, reaching up to 350 μm.[11]

The present work was motivated by the increasing experimental activity in the direction of spin injection and manipulation in Si,[9–15] as well as by arguments for advantages of spin transport in Si.[16] Based on density-functional calculations we examine the possibility of direct spin injection from Fe into Si, with the Schottky barrier of Si used as the necessary tunneling barrier. We focus on idealized epitaxial, atomically flat Fe/Si(001) interfaces. After briefly presenting the magnetic structure of the Fe/Si interface, we discuss the tunneling properties of Si based on the concept of complex band structure. We then show that spin injection is possible and can be tuned by adjusting the Fermi level E_F in the band gap of Si in the tunneling region, or by straining Si in the injection region in order to cut off satellite contributions. We further discuss the so-called $\bar{\Gamma}$-point rule for increased injection efficiency and show that, in the case of Fe/Si, it is harder to satisfy than in Fe/GaAs.

II. METHOD AND DETAILS OF CALCULATION; LIMITATIONS OF APPROACH

The electronic structure of the junctions was calculated within the local (spin) density approximation [L(S)DA] to density-functional theory. The Kohn-Sham equations were solved using the screened Korringa-Kohn-Rostoker (KKR) Green function method.[17] A nonrelativistic treatment was chosen, as it is known that relativistic corrections result in a reduction of the calculated semiconductor gaps within the LDA. The atomic sphere approximation was used in most cases, except in particular tests which were performed with a full potential treatment. The conductance was calculated in the zero-bias limit within a Landauer-Büttiker approach adjusted to the KKR Green function method.[18]

The self-consistent electronic structure of the junction was calculated using the decimation technique[19] for the consideration of the half-infinite leads. An angular momentum cutoff of $\ell_{\max}=2$ was used. The details of the electronic structure that are important here change only little between $\ell_{\max}=2$ and $\ell_{\max}=3$; for example, the spin moment of bcc Fe changes by less than 5%. However, an angular momentum cutoff of $\ell_{\max}=3$ was necessary[18] for the calculation of the conductance matrix elements.

The Fe/Si(001) interface was taken to be ideal (atomically flat). Contrary to the wave functions, the perturbation of the

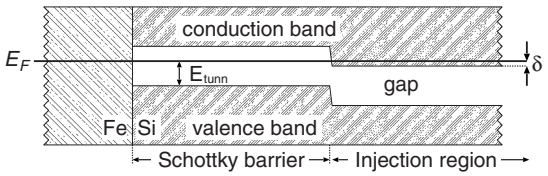

FIG. 1. Schematic representation of the band diagram at the Fe/Si interface used in the calculations.

potentials dies out relatively fast with the distance from the interface. Within a finite region of two atomic layers around the interface, the potentials are perturbed from their bulklike values and calculated self-consistently by sandwiching five layers of Si between two Fe leads. This way also provides the band alignment between Fe and Si. Subsequently the half-infinite Si lead is constructed by maintaining the potentials only up to the middle of the junction (left Fe lead and Si up to third layer), and repeating the potential of the third Si layer (which is considered already bulklike) ad infinitum by use of the decimation technique. The decimation technique is also used to produce the half-infinite, bulklike Fe lead. The same method has been applied in previous works on Fe/GaAs and Fe/ZnSe.[20,21]

We consider the following external parameters that are involved in an injection experiment (see also Fig. 1). First, the Schottky barrier has a thickness of N_{SB} layers and a height determined by the band alignment of Si with respect to the Fermi level of Fe. Experimentally, this can be adjusted by appropriate doping or by a gate voltage. In the calculations, this is simulated by adding an appropriate constant shift to the Si potentials up to N_{SB} so that within the barrier, the bands are shifted and E_F (which is fixed by the Fe lead) falls at a desired position between the valence band and conduction-band edges, E_v and E_c: $E_F=E_v+E_{tunn}$. In this step the first two Si layers at the interface are excluded, as it is considered that their electronic structure will be mainly affected by their proximity to Fe. Second, after the barrier region the band alignment must be such that the injected electrons arrive in the Si valence band. Experimentally the appropriate band alignment can also be adjusted by a gate voltage or by doping. Here, it is again accounted for by adding a proper energy constant to the potentials of all Si layers from $N_{SB}+1$ and so on, so that E_F falls slightly in above E_c: $E_F=E_c+\delta$. In the present work $\delta=28$ meV (2 mRyd) was used except where otherwise indicated.

A few comments are in order on the chosen band diagram. First, in experiment a Schottky barrier will possibly have a different, less abrupt shape. We defer this question for Sec. VI, after the discussion has revealed the effect of the positioning of E_F in the gap. Second, the chosen value of $\delta=28$ meV can be perhaps reasonable for GaAs, but would probably result in an unrealistically high carrier concentration in Si due to the high Si effective mass. This choice helps in visualizing and understanding the current distribution in the surface Brillouin zone (SBZ). In Sec. V we also show calculations with δ up to 1.4 meV, which in fact reveal a qualitative change of injection efficiency.

It is well known that local density-functional theory (as is the LDA or the generalized gradient approximation) underestimates the gap in semiconductors and insulators; in the present calculations the Si band gap is found to be approximately 0.38 eV. Thus, the values of tunneling conductance obtained within density-functional calculations can only provide qualitative understanding, including trends, but not quantitatively correct results. Qualitatively, the underestimated band gap in the tunneling region can be partly compensated by increasing the barrier thickness N_{SB}. Here, N_{SB} was varied up to 60 Si layers.

Especially for the calculation of the bulk Si band structure (including the complex band structure), significant quantitative improvement can be achieved by using an orthogonalized plane wave method with pseudopotentials fitted to optical excitation experiments. Here we followed such a method with the parameters taken from Ref. 22; in the presentation of the results we indicate when this method has been used.

Furthermore we note that an atomically flat interface is, at this point, an idealization. In an experiment, interface roughness and disorder are hard to avoid, and some form of iron silicide will be present at the interface. However, it cannot be excluded that good quality, atomically almost flat interfaces can, in principle, be made, as has been achieved in Fe/MgO junctions. For example, experiments[23] show well-defined interlayer exchange coupling on Fe/Si/Fe trilayers, which is an indication of improved interface quality. Moreover, the parameter space becomes simply too big if many possibilities of interface structure are to be calculated. Since modern experimental techniques allow for a detailed imaging of the interface structure,[24] it is possible to relate further calculations to such experimental input. In Sec. VI we point out which calculated properties are specific to the idealization of a flat interface.

Finally we comment on the lattice mismatch of Fe and Si. The Si lattice constant (5.43 Å) is approximately twice the one of Fe (2.87 Å) with a mismatch of about 5%. We adopt the Si lattice constant for the calculation (the in-plane unit cell accommodates now two Fe atoms per Fe layer) to simulate the situation where a thin film of Fe is in contact with a thick Si barrier. The stress on the Fe contacts will be appreciable, but it is sufficient that Fe retains the prescribed epitaxial structure for only a few layers for the conclusions to be correct. This has been demonstrated in calculations on Fe/MgO/Fe junctions,[25] where it was shown that the transport properties depend on the structure of the Fe lead only close to the interface: even if Fe becomes amorphous a few layers away from the interface, the spin filtering properties practically do not change. However, the choice of lattice constant does affect the moments significantly, and therefore tests on interface relaxation and tetragonalization were made, as we discuss in Sec. III.

III. SPIN MOMENTS AT THE INTERFACE; EFFECT OF LATTICE CONSTANT

The spin moment of bulk Fe was found not to change too much with lattice constant: a moment reduction of 12% was calculated at the Si lattice constant compared to the result at the Fe lattice constant. However, the change of the moments at the interface is appreciable. At the Si lattice constant, the

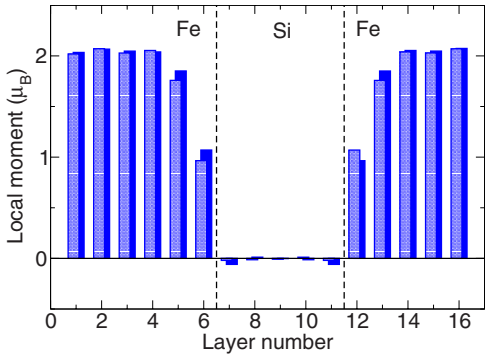

FIG. 2. (Color online) Atom-resolved spin moments close to the interface in a Fe/Si/Fe(001) junction, calculated at the Si lattice parameter. Evidently the Fe moments at the interface are strongly suppressed. The two values for each layer correspond to the two inequivalent atoms.

moments of the interface Fe atoms are reduced to approximately half their bulk value, as is shown in Fig. 2. This effect, previously reported, e.g., in Ref. 26, is not present in calculated junctions at the Fe lattice constant, where the interface Fe moments are not suppressed at all.

The magnetic structure was further tested by calculating a finite slab of four layers Fe/4 layers Si/4 layers Fe with a full potential treatment and $\ell_{\max}=3$. Here the in-plane lattice constant of Si was adopted, while the Fe layers were allowed to assume an optimal c/a ratio, and the interlayer distance at the interface was relaxed. No qualitative differences were found compared to the results using the Si lattice constant for a and c: the strong suppression of the moments was still present.

We conclude that a strong suppression of the Fe interface moment is unavoidable if the in-plane lattice parameter of Si(001) is adopted. Interestingly, this does not qualitatively affect the transport properties that interest us here, in particular it does not kill (or even suppress) the spin polarization of the injected current. This was found by test calculations of spin injection in a Fe/Si(001) junction using the Fe lattice parameter (whence the moments at the interface where not compromised).

IV. ROLE OF SILICON REAL AND COMPLEX BAND STRUCTURE

Silicon has an indirect band gap. The valence band has a maximum at the Γ point ($\vec{k}=0$), while the conduction band has six equivalent degenerate minima at $\vec{k}=(\pm k_0,0,0)$, $(0,\pm k_0,0),(0,0,\pm k_0)$ with $k_0\approx 0.852\pi/a$ (a is the lattice parameter). These properties are most important for a qualitative discussion of the tunneling conductance and electron injection.

The results of this section were obtained by using pseudopotentials fitted to optical transitions.[22] The band structure of Si around the gap is shown in Fig. 3. The conduction band around the minima forms six ellipsoidal "pockets" of highly anisotropic effective mass, as shown schematically in Fig. 4. Electron injection takes place into these pockets; if the junction growth is along the [001] direction, then the pockets are projected in five conductance hot spots on the two-dimensional (001) surface Brillouin zone (Fig. 4). One of these is at $\vec{k}_\parallel=0$, while the other four are equivalent and form a satellite structure. (We denote by $\vec{k}_\parallel$ the projection of the Bloch $\vec{k}$ vector on the surface Brillouin zone.)

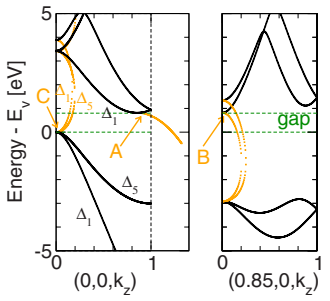

FIG. 3. (Color online) Real and complex band structure of Si along the k_z direction at $\vec{k}_\parallel=0$ (left) and $\vec{k}_\parallel=(0.85,0)(2\pi/a)$ (right). Black lines stand for real bands as $E=E(k_z)$; orange (or gray) lines stand for complex bands as $E=E(k_z+i\kappa)$. The effective mass anisotropy at the six pockets of the conduction-band edge, $k_{x,y,z}\approx\pm 0.85(2\pi/a)$, evidently results in a quite different curvature of the complex bands departing from these (indicated by arrows). Therefore, when E_F is close to the conduction-band edge, the tunneling is dominated by the contributions at the four equivalent points $\vec{k}_\parallel\approx(\pm 0.85,0)(2\pi/a)$, $\vec{k}_\parallel\approx(0,\pm 0.85)(2\pi/a)$. The symmetry of the bands is also indicated (Δ_1 and Δ_5). (More complex bands, irrelevant for the discussion, have been omitted.)

The pocket structure is highly important also for the tunneling properties. Setting the z axis along the [001] epitaxy direction, the tunneling wave function at E_F depends on the

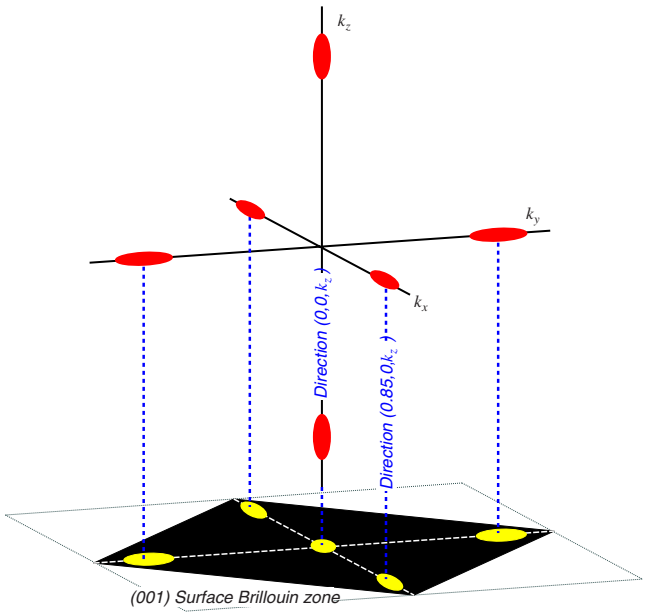

FIG. 4. (Color online) Schematic representation of the six equivalent Si conduction-band "pockets." When these are projected on the two-dimensional (001) surface Brillouin zone, five hot spots for conductance in the [001] direction arise: one central (at $\vec{k}_\parallel=0$) and four equivalent satellites.

decay parameter $\kappa(\vec{k}_\parallel;E_F)$ as $\psi(\vec{r})\sim\exp(-\kappa z)$. The set of $\kappa(\vec{k}_\parallel;E)$ forms the so-called complex band structure; evidently, the lowest values of κ are responsible for the highest tunneling current. The value of $\kappa(\vec{k}_\parallel;E_F)$ depends on the proximity of E_F to the Bloch eigenvalues $E(\vec{k}_\parallel;k_z)$ of the same $\vec{k}_\parallel$ in the conduction or valence band, and on the curvature of $E(\vec{k}_\parallel;k_z)$ with respect to k_z (i.e., the effective mass in the k_z direction). Thus the effective mass anisotropy of the pockets in the Si tunneling barrier has consequences that we now discuss.

Figure 3 shows the complex (and real) band structure in the [001] (k_z) direction for two different values of $\vec{k}_\parallel$: $\vec{k}_\parallel=0$ and $\vec{k}_\parallel=(k_0,0)$; the latter corresponds to one of the aforementioned "satellite" conductance hot spots. Arrows A and B indicate the pocket positions, and the effective mass anisotropy is evident. The indicated pocket in the left panel (arrow A) has its long axis along the k_z direction. The complex band (in orange, arrow A) departing from the edge of this pocket has a small curvature (as it is along the long axis of the pocket), leading quickly to high values of κ for $E_F<E_c$. On the other hand, the pocket indicated in the right panel (arrow B) has its long axis oriented in the k_x direction. Here, the complex band along k_z inherits a large curvature from the small axis of the pocket, and the value of κ remains relatively small for $E_F<E_c$.

Consequently, when E_F is in the gap but close to the conduction-band edge, the tunneling current through the satellite positions dominates, while the tunneling current through the Brillouin zone center is small. However, if E_F is lowered closer to the valence-band edge, a different contribution from the Brillouin zone center becomes more important, marked by arrow C in Fig. 3. This comes about via the complex band of Δ_1 symmetry arising from the valence-band maximum.

The picture becomes more complete if the full (001) surface Brillouin zone is scanned for the lowest branch of $\kappa(\vec{k}_\parallel;E_F)$ at different values of E_F. Figure 5 shows two such "complex Fermi surfaces:" (A) one for $E_F=E_v+0.725$ eV (close to E_c), and (B) one for $E_F=E_v+0.325$ eV (just a little lower than the middle of the gap). Brighter colored regions correspond to lower values of κ. In the first case, as E_F is close to E_c, the parts of the complex Fermi surface at the satellite hot spots show the lowest κ. As we shall see in the next section, conductance calculations also show that these regions dominate the tunneling current for an analogous choice of E_F. In the second case shown in Fig. 5, the minimum of κ is found at the Brillouin zone center. Then the tunneling contribution at $\vec{k}_\parallel=0$ dominates if the Schottky barrier is thick.

We close this section with the conclusion that the indirect gap of Si lends features to the complex band structure which are qualitatively different than direct-gap compounds, as GaAs, ZnSe, or MgO. Contrary to all these direct-gap materials, where the complex band of Δ_1 symmetry at the Brillouin zone center gives the dominant contribution irrespective of the exact position of E_F, in Si the positioning of E_F can make a stark difference. This effect can have consequences for all physical properties which depend on the complex band structure. Particularly in spintronics applications it can affect spin injection, tunneling magnetoresistance, but also ground-state properties such as interlayer exchange coupling.[27]

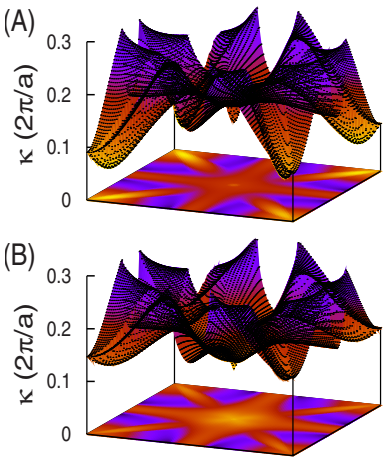

FIG. 5. (Color online) Complex band structure [decay parameter $\kappa(\vec{k}_\parallel;E_F)$] in the band gap of Si in the [001] direction for $E_F=E_v+0.725$ eV (a) and at $E_F=E_v+0.325$ eV (b). In the former case, E_F is close to the conduction-band edge, and the four equivalent contributions at $\vec{k}_\parallel\approx(\pm0.85,0)(2\pi/a)$ and $\vec{k}_\parallel\approx(0,\pm0.85)(2\pi/a)$ dominate the tunneling; in the latter case, E_F is located a little lower than the middle of the gap, and the decay parameter at $\vec{k}_\parallel=0$ is lowest. Only the lowest branch of $\kappa(\vec{k}_\parallel)$ is shown. Brighter shaded regions correspond to lower κ and more efficient tunneling.

V. TOTAL AND SPIN-DEPENDENT CONDUCTANCE; CURRENT POLARIZATION

We now proceed to the presentation and discussion of the *ab initio* results on the conductance and current polarization. We start by commenting on the effect of the underestimation of the gap in the density-functional theory. The conclusions of Sec. IV are qualitatively still valid, but now, within the barrier, the possible choice of E_c-E_F is more limited (otherwise E_F will enter the valence band). This results in an overestimation of the relative contribution of the satellites to the current. As the calculations show, the satellites dominate the current even when E_F is at the midgap position; hence, calculated results at midgap are expected to be closer to a realistic situation of shallow tunneling close to E_c. An overestimated proximity of E_F to the the valence band is necessary so for the Brillouin zone center contribution to prevail. Moreover, the decay parameters and exponential falloff of the conductance with barrier thickness are underestimated.

A. Total conductance

Figure 6 shows the calculated conductance per two-dimensional interface unit cell as a function of the barrier thickness. Results for two different positions of E_F are presented: midgap tunneling ($E_F=E_v+190$ meV) and shallow tunneling close to the valence-band edge ($E_F=E_v+28$ meV). The partial contributions of the region around the Brillouin zone center and the satellites are also shown. An exponential decay with thickness is characteristic of tun-

neling, and the slope of the curve in a logarithmic scale is proportional to the decay parameter.

In the case of midgap tunneling [Fig. 6(a)] it is clear that the satellite contribution dominates at all thicknesses, being practically equal to the total conductance, while the central contribution to the total current is insignificant. While the slope of the satellite part of the conductance is constant, reflecting a single decay parameter κ_{sat}, the central contribution gradually changes slope; after a thickness of about 20 layers, only the Δ_1 contribution remains around $\vec{k}_{\parallel}=0$, with a decay parameter $\kappa_1 \approx \kappa_{\mathrm{sat}}$.

The behavior in the case of shallow tunneling, closer to the valence-band edge [Fig. 6(b)], is analogous. Here, however, the low positioning of E_F evidently results in $\kappa_1 < \kappa_{\mathrm{sat}}$ (see also Fig. 3). Thus after a thickness of 35 layers the central contribution prevails and dominates the tunneling current.

In both cases we also observe that for small thicknesses (five layers), the satellite contribution is much stronger than the central one. Apparently there is a much stronger coupling between the Fe and Si states at the satellite positions in the Brillouin zone. At this point we have no intuitive explanation for this effect.

B. Spin-dependent conductance and current polarization

The spin polarization of the current is defined as

$$P = \frac{I_\uparrow - I_\downarrow}{I_\uparrow + I_\downarrow}, \tag{1}$$

where $I_\uparrow$ and $I_\downarrow$ are the current of majority-spin and minority-spin carriers, respectively. The difference between $I_\uparrow$ and $I_\downarrow$ arises mainly from the spin-dependent scattering at the Fe/Si interface (which gives rise to spin-dependent tunneling), due to the difference in coupling of Fe wave functions of different spin to Si wave functions at the interface.

The calculated current polarization as a function of barrier thickness is shown in Fig. 7. Again, two cases are presented, corresponding to (A) midgap tunneling ($E_F=E_v+190$ meV within the barrier) and (B) shallow tunneling close to the valence-band edge ($E_F=E_v+28$ meV within the barrier), as was the case in Fig. 6. These were chosen as representative of different physical situations, where the dominant contribution to the current stems from different parts of the Brillouin zone. In both cases the band alignment in the injection region (i.e., after the barrier) was chosen such that $\delta := E_F - E_c = 28$ meV. Apart from the total current polarization, two contributions of special interest are shown: one at exactly the $\bar{\Gamma}$ point ($P_{\bar{\Gamma}}$) and one integrated around the $\bar{\Gamma}$ point (P_{cntr}). In terms of the $\vec{k}_{\parallel}$-resolved current, $I_\uparrow(\vec{k}_{\parallel})$ and $I_\downarrow(\vec{k}_{\parallel})$, these contributions are defined as

$$P_{\bar{\Gamma}} = \frac{I_\uparrow(\vec{k}_{\parallel}=0) - I_\downarrow(\vec{k}_{\parallel}=0)}{I_\uparrow(\vec{k}_{\parallel}=0) + I_\downarrow(\vec{k}_{\parallel}=0)} \tag{2}$$

and

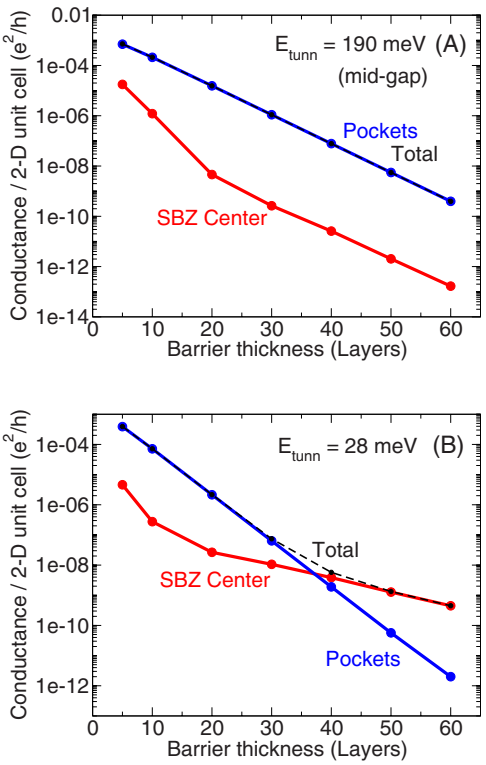

FIG. 6. (Color online) Conductance per two-dimensional unit cell as a function of the Schottky barrier thickness for (a) midgap tunneling ($E_{\mathrm{tunn}}=190$ meV) and (b) shallow tunneling close to the valence band ($E_{\mathrm{tunn}}=28$ meV). The contributions of the region around the SBZ center (integrated around the $\bar{\Gamma}$ point) and the satellites are shown separately.

$$P_{\mathrm{cntr}} = \frac{\int d^2k_{\parallel}[I_\uparrow(\vec{k}_{\parallel}) - I_\downarrow(\vec{k}_{\parallel})]}{\int d^2k_{\parallel}[I_\uparrow(\vec{k}_{\parallel}) + I_\downarrow(\vec{k}_{\parallel})]}, \tag{3}$$

where the latter integration takes place in the central part of the Brillouin zone where the current is nonzero (the central hot spot of Fig. 4).

We first discuss Fig. 7(a). Here the polarization is dominated by the satellite contributions for all thicknesses, as the current at the SBZ center is negligible [cf. Figure 6(a)]. The polarization is rather insensitive to the barrier thickness, being around $P=60\%$. In Fig. 7(c), the $\vec{k}_{\parallel}$-resolved conductance is shown for both spin directions in the full SBZ for a barrier thickness of $N_{\mathrm{SB}}=40$ monolayers. Evidently the SBZ center has a negligible contribution, while the conductance at the satellite positions is higher for majority spin than for minority spin by approximately a factor of two. However, the contribution at exactly the $\bar{\Gamma}$ point shows an interesting behavior, almost reaching the ideal $P_{\bar{\Gamma}}=100\%$; the integrated value around $\bar{\Gamma}$, $P=P_{\mathrm{cntr}}$, is lower. Before analyzing this we discuss Fig. 7(b). Here, for small barrier thicknesses, the current is dominated by the satellites, which yield a polarization of about 50%. However for larger thicknesses, only the central contribution to the current is of significance [cf. Figure 6(b)].

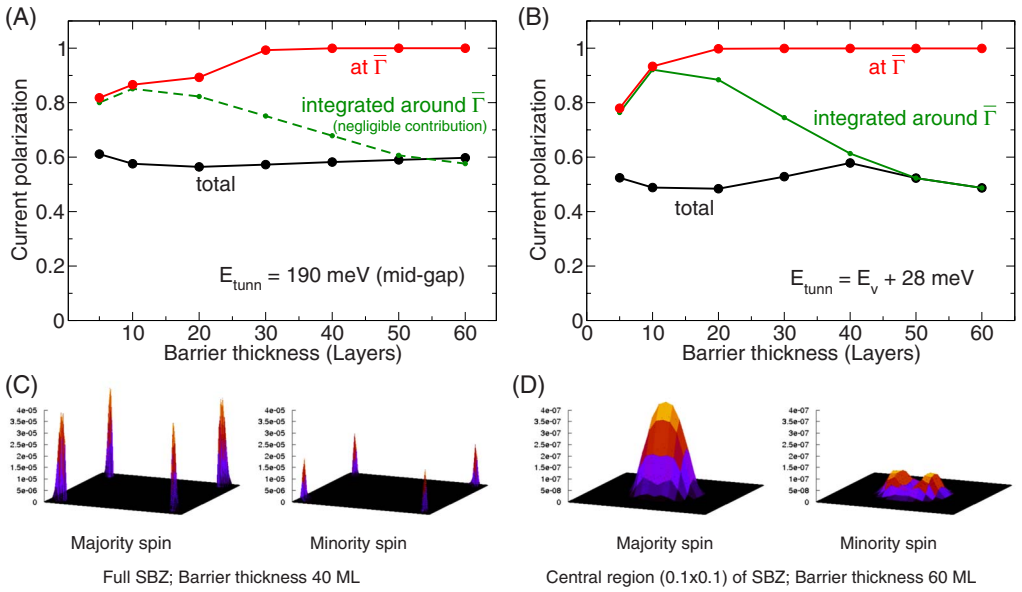

FIG. 7. (Color online) (A and B) Current polarization as a function of the barrier thickness for an injection energy of δ=28 meV and for a tunneling energy E_{tunn} at midgap (a) and at 28 meV (b). Shown are the total polarization (see Eq. (1)), polarization at $\bar{\Gamma}$ (Eq. (2)), and the integrated polarization at the central hot spot (Eq. (3)). (c): Conductance as a function of $\vec{k}_{\parallel}$ in the SBZ for a barrier thickness of 40 layers in the case of E_{tunn} at midgap. The SBZ center contribution is insignificant next to the satellites' contribution. (d): Similar as in (c), but for a barrier thickness of 60 layers in the case of E_{tunn}=28 meV. Here the 0.1×0.1 central part of the SBZ is focused on, since the satellites are negligible. A double-peak structure, with a dip at $\bar{\Gamma}$, is evident for minority spin.

Already at a thickness of 50 monolayers, $P=P_{\text{cntr}}$. Again we see that, exactly at the SBZ center, $P_{\bar{\Gamma}} \approx 100\%$.

In order to elucidate the situation at the SBZ center we show in Fig. 7(d) the $\vec{k}_{\parallel}$-resolved conductance focused in the region around the $\bar{\Gamma}$ point, for the case of shallow tunneling ($E_F=E_v+28$ meV in the barrier) and a barrier thickness of 60 monolayers. The majority-spin conductance shows a single-peak structure with a maximum at the $\bar{\Gamma}$ point. On the other hand, the minority-spin conductance as a function of $\vec{k}_{\parallel}$ has a double-peak structure around $\vec{k}_{\parallel}=0$, with a pronounced dip at exactly $\vec{k}_{\parallel}=0$, which is responsible for the value $P_{\bar{\Gamma}} \approx 100\%$.

Obviously the $\bar{\Gamma}$ point enjoys special properties. This "$\bar{\Gamma}$-point rule" has been observed and explained in previous works[20,21,28,29] on spin injection from Fe into direct gap semiconductors in the zinc-blende structure (GaAs, ZnSe, InAs). The reason is traced back to the symmetry of the wave functions at E_F, at $\vec{k}_{\parallel}=0$. The semiconductor wave functions at $\vec{k}_{\parallel}=0$ have Δ_1 symmetry, which for Fe is present among the majority spin wave functions but absent among the minority spin wave functions at E_F, at least in the [001] direction. This symmetry mismatch of the Fe minority spin to the semiconductor wave functions results in almost total reflection so that the current is almost 100% polarized. Departing from $\vec{k}_{\parallel}=0$, the Si bands acquire a mixed character, such that the Fe Δ_5 states (of d_{xz} and d_{yz} character), coupling to the Si Δ_5 complex band in the barrier, can also tunnel into the conduction band after the barrier. Then the minority-spin transmission rises, as is shown in Fig. 7(d).[30] Note that no such special point appears in the satellite hot spots although their centers lie on the high-symmetry directions $\bar{\Gamma}-\bar{M}$ (along the cubic x and y axes).

This behavior close to $\bar{\Gamma}$ is typical also for smaller thicknesses and for different tunneling energies, therefore the polarization $P_{\bar{\Gamma}}$ reaches high values also in Fig. 7(a). We infer that the integrated spin polarization can be increased if two requirements are fulfilled: (i) the central hot spot must be as small as possible; and (ii) the satellite contributions must be made negligible. Both can, in principle, be fulfilled, as we now discuss.

Concerning requirement (i), the radius k_{max} of the hot spots depends on the injection energy $\delta=E_F-E_c$ in the injection region as $\delta \sim k_{\text{max}}^2$. However δ is adjustable, e.g., by tuning the gate voltage of the doping concentration. In particular for Si, due to the high effective mass the value δ =28 meV used in the calculations hitherto is rather high and was chosen in order to reveal the structure of the $\vec{k}_{\parallel}$-resolved conductance, as already commented in Sec. II. By choosing a smaller δ, the SBZ center is approached more and more, and the integrated polarization P_{cntr} rises. This is demonstrated in Fig. 8. At δ=1.4 meV, P_{cntr} is already over 90%, while in the limit $\delta=0$ we obtain $P_{\text{cntr}} \to P_{\bar{\Gamma}} \approx 100\%$. Interestingly this results in a "zero-gate anomaly" (if δ is considered to be a gate voltage) demonstrated in the inset of Fig. 8, where P_{cntr} is shown as a function of δ at a barrier thickness of 60 layers. Evidently the polarization drops abruptly with increasing δ. Note that controlled injection at about $\delta \approx 1$ meV requires low temperatures to avoid thermal broadening since 1 meV corresponds to 11.6 K. In this respect, the $\bar{\Gamma}$-point rule is easier satisfied in direct-gap semiconductors, where due to

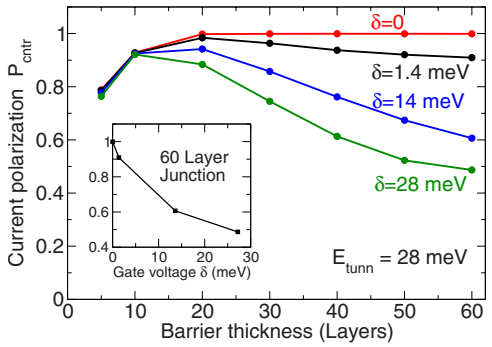

FIG. 8. (Color online) Polarization around the $\bar{\Gamma}$ point, P_{cntr} [see Eq. (3)], for small values of the injection energy δ. Inset: Zero-gate "anomaly" of the polarization for a 60-layer barrier.

the low effective mass the $\vec{k}_{\parallel}$-resolved current is confined to a tiny region around $\bar{\Gamma}$ also at higher δ.

Although Fig. 8 shows results for shallow tunneling at $E_{\mathrm{tunn}}=28$ meV, the behavior of P_{cntr} is entirely analogous at higher E_{tunn}, e.g., in the case of midgap tunneling. Qualitatively, what changes is only the relative importance of the satellite contributions to the central contribution.

This brings us to the discussion of requirement (ii). Is it possible to cut off the satellites? We already saw that this happens as the Fermi level approaches the valence band in the barrier region if the barrier is thick enough. However there is also another possibility, namely by tetragonally straining Si. In tetragonally strained Si the degeneracy of the six conduction pockets is lifted. In the case that $c/a<1$, the two pockets along the c axis (i.e., z axis along the epitaxial direction in the presented geometry) are lowered in energy compared to the four pockets along the x and y axes.[31] Even a moderate strain of 0.5% ($c/a=0.995$) was calculated to lift the degeneracy by approximately 30 meV. As long as the injection energy δ is kept under this limit, only the central conductance hot spot will be populated in the injection region, while the satellites will be cut off.

VI. SUMMARY AND CONCLUDING REMARKS; OUTLOOK

Electrical injection from Fe into Si(001) through a Schottky barrier has been shown to be theoretically possible. A detailed discussion of the complex band structure of Si in the [001] direction has revealed qualitative differences in the tunneling process compared to direct-gap semiconductors. As a result of the complex band structure, the current and polarization contributions at different conduction pockets have been shown to vary very strongly depending on the Schottky barrier thickness and the position of the Fermi level in the barrier. Depending on these parameters, the injection efficiency has been found to range between 50% and 100%.

In the calculations a particular junction setup was assumed, including a number of approximations or idealizations. One approximation lies in the shape of the Schottky barrier. It was assumed that the transition from the Schottky region to the injection region is abrupt. However, except for the case of very precise interface engineering (e.g., with an appropriate doping profile), the transition to the injection region is more gradual. This would result in position-dependent decay parameters, with the central part of the SBZ providing better tunneling close to the interface (where the middle of the gap should be at E_F) and the satellite positions being more efficient close to the injection region (where E_c is lowered toward E_F). Thus, overall, either the SBZ center or the satellites would dominate the tunneling current, depending on the exact shape of the barrier. The barrier shape can also significantly affect spin extraction (from Si into Fe) if localized bands are formed next to the Schottky barrier due to the doping profile.[32]

An idealization was that of an atomically flat Fe/Si interface, with the in-plane lattice structure unaltered. While possible in principle, in practice it can prove hard to achieve. If the two-dimensional periodicity is violated at the interface, then the most severe consequence (with regard to the results presented in the present work) is expected to be the absence of excellent spin filtering at the $\bar{\Gamma}$ point. As was mentioned earlier, the extreme current polarization stems from the symmetry mismatch of the Si and minority-spin Fe wave functions at $\vec{k}_{\parallel}=0$. Such symmetry arguments do not hold any more in the absence of perfect interface epitaxy. It has been shown,[29] e.g., in Fe/InAs(001) spin injection (where the same principle holds), that increasing interface disorder leads to a decrease in current polarization. However, a few perfectly epitaxial Fe layers should be enough for a symmetry-induced polarization. This has been found in an analogous case of symmetry-induced polarization in Fe/MgO/Fe(001) tunnel junctions.[25] Furthermore, it should be noted that since an MgO barrier is known to be selective of the Δ_1 states at $\vec{k}_{\parallel}=0$, it can also be used to increase the efficiency in spin injection experiments. Efficient spin injection has been found in FeCo/MgO/GaAs and FePt/MgO/GaAs junctions,[7] while work in this direction has been reported also for FeCoB/MgO/Si junctions.[15]

A reduction of efficiency can also be caused by the formation of iron silicide at the interface, which can sometimes lead to noncollinear magnetic ordering. This can be avoided by inserting a nonmagnetic metal between Fe and Si (as was done, e.g., in Refs. 10 and 11); calculations on such junctions will be the object of future work.

ACKNOWLEDGMENTS

It is a pleasure to thank George Kioseoglou and Ian Appelbaum for enlightening discussions on the current state of the art in spin injection experiments in Si, and Stefan Blügel for his support and help throughout this project.

[1] S. Datta and B. Das, Appl. Phys. Lett. **56**, 665 (1990).
[2] G. Schmidt, D. Ferrand, L. W. Molenkamp, A. T. Filip, and B. J. van Wees, Phys. Rev. B **62**, R4790 (2000).
[3] E. I. Rashba, Phys. Rev. B **62**, R16267 (2000).
[4] A. Fert and H. Jaffrès, Phys. Rev. B **64**, 184420 (2001).
[5] A. T. Hanbicki, B. T. Jonker, G. Itskos, G. Kioseoglou, and A. Petrou, Appl. Phys. Lett. **80**, 1240 (2002).
[6] O. M. J. van't Erve, G. Kioseoglou, A. T. Hanbicki, C. H. Li, B. T. Jonker, R. Mallory, M. Yasar, and A. Petrou, Appl. Phys. Lett. **84**, 4334 (2004).
[7] X. Jiang, R. Wang, R. M. Shelby, R. M. Macfarlane, S. R. Bank, J. S. Harris, and S. S. P. Parkin, Phys. Rev. Lett. **94**, 056601 (2005); A. Sinsarp, T. Manago, F. Takano, and H. Akinaga, Jpn. J. Appl. Phys., Part 2 **46**, L4 (2007).
[8] Xiaohua Lou, Christoph Adelmann, Scott A. Crooker, Eric S. Garlid, Jianjie Zhang, K. S. Madhukar Reddy, Soren D. Flexner, Chris J. Palmstrom, and Paul A. Crowell, Nat. Phys. **3**, 197 (2007).
[9] I. Appelbaum, B. Huang, and D. J. Monsma, Nature (London) **447**, 295 (2007).
[10] Biqin Huang, Lai Zhao, Douwe J. Monsma, and Ian Appelbaum, Appl. Phys. Lett. **91**, 052501 (2007).
[11] Biqin Huang, Douwe J. Monsma, and Ian Appelbaum, Phys. Rev. Lett. **99**, 177209 (2007); Biqin Huang and Ian Appelbaum, Phys. Rev. B **77**, 165331 (2008).
[12] O. M. J. van 't Erve, A. T. Hanbicki, M. Holub, C. H. Li, C. Awo-Affouda, P. E. Thompson, and B. T. Jonker, Appl. Phys. Lett. **91**, 212109 (2007).
[13] B. T. Jonker, G. Kioseoglou, A. T. Hanbicki, C. H. Li, and P. E. Thompson, Nat. Phys. **3**, 542 (2007).
[14] B. C. Min, J. C. Lodder, R. Jansen, and K. Motohashi, J. Appl. Phys. **99**, 08S701 (2006).
[15] T. Uhrmann, T. Dimopoulos, H. Brückl, V. K. Lazarov, A. Kohn, U. Paschen, S. Weyers, L. Bär, and M. Rührig, J. Appl. Phys. **103**, 063709 (2008).
[16] Igor Žutić, Jaroslav Fabian, and Steven C. Erwin, Phys. Rev. Lett. **97**, 026602 (2006).
[17] K. Wildberger, R. Zeller, and P. H. Dederichs, Phys. Rev. B **55**, 10074 (1997); N. Papanikolaou, R. Zeller, and P. H. Dederichs, J. Phys.: Condens. Matter **14**, 2799 (2002).
[18] P. Mavropoulos, N. Papanikolaou, and P. H. Dederichs, Phys. Rev. B **69**, 125104 (2004).
[19] B. Wenzien, J. Kudrnovsky, V. Drchal, and M. Sob, J. Phys.: Condens. Matter **1**, 9893 (1989).
[20] O. Wunnicke, P. Mavropoulos, R. Zeller, P. H. Dederichs, and D. Grundler, Phys. Rev. B **65**, 241306(R) (2002).
[21] O. Wunnicke, Ph. Mavropoulos, R. Zeller, and P. H. Dederichs, J. Phys.: Condens. Matter **16**, 4643 (2004).
[22] Marvin L. Cohen and T. K. Bergstresser, Phys. Rev. **141**, 789 (1966).
[23] D. E. Bürgler, M. Buchmeier, S. Cramm, S. Eisebitt, R. R. Gareev, P. Grünberg, C. L. Jia, L. L. Pohlmann, R. Schreiber, M. Siegel, Y. L. Qin, and A. Zimina, J. Phys.: Condens. Matter **15**, S443 (2003).
[24] Thomas J. Zega, Aubrey T. Hanbicki, Steven C. Erwin, Igor Zutic, George Kioseoglou, Connie H. Li, Berend T. Jonker, and Rhonda M. Stroud, Phys. Rev. Lett. **96**, 196101 (2006).
[25] C. Heiliger, M. Gradhand, P. Zahn, and I. Mertig, Phys. Rev. Lett. **99**, 066804 (2007).
[26] M. Freyss, N. Papanikolaou, V. Bellini, R. Zeller, and P. H. Dederichs, Phys. Rev. B **66**, 014445 (2002).
[27] Interlayer exchange coupling of ferromagnetic layers separated by an insulator depends on the insulator complex band structure. See, e.g., P. Bruno, Phys. Rev. B **49**, 13231 (1994).
[28] Ph. Mavropoulos, O. Wunnicke, and P. H. Dederichs, Phys. Rev. B **66**, 024416 (2002).
[29] M. Zwierzycki, K. Xia, P. J. Kelly, G. E. W. Bauer, and I. Turek, Phys. Rev. B **67**, 092401 (2003).
[30] As was discussed previous papers on Fe/GaAs and Fe/ZnSe (Refs. 20, 21, and 28) the polarization at $\vec{k}_{\|}=0$ may be less than 100%, because the point group rotational symmetry around the [001] axis is C_{4v} for Fe but C_{2v} for the zinc-blende or diamond structure. Thus, minority-spin Fe states of $\Delta_{2'}$ symmetry (d_{xy} character) at E_F can weakly couple to semiconductor states of Δ_1 symmetry. This weak coupling was found (Ref. 21) to result in resonant interface states penetrating the Schottky barrier, which under certain conditions reduced $P_{\bar{\Gamma}}$ by 10–20%. Such a strong contribution from interface states is not observed in Fe/Si(001).
[31] Such strain is experimentally feasible, and has the additional advantage of achieving improved mobility. See, e.g., D. Buca, B. Hollander, S. Feste, St. Lenk, H. Trinkaus, S. Mantl, R. Loo, and M. Caymax, Appl. Phys. Lett. **90**, 032108 (2007).
[32] H. Dery and L. J. Sham, Phys. Rev. Lett. **98**, 046602 (2007).